Article

TRANSPARENT PROCESS

EMBO reports

Wnt directs the endosomal flux of LDL-derived cholesterol and lipid droplet homeostasis

Cameron C Scott[1], Stefania Vossio[1], Fabrizio Vacca[1], Berend Snijder[2,†], Jorge Larios[1], Olivier Schaad[1], Nicolas Guex[3], Dmitry Kuznetsov[3], Olivier Martin[3], Marc Chambon[4], Gerardo Turcatti[4], Lucas Pelkmans[2] & Jean Gruenberg[1,*]

Abstract

The Wnt pathway, which controls crucial steps of the development and differentiation programs, has been proposed to influence lipid storage and homeostasis. In this paper, using an unbiased strategy based on high-content genome-wide RNAi screens that monitored lipid distribution and amounts, we find that Wnt3a regulates cellular cholesterol. We show that Wnt3a stimulates the production of lipid droplets and that this stimulation strictly depends on endocytosed, LDL-derived cholesterol and on functional early and late endosomes. We also show that Wnt signaling itself controls cholesterol endocytosis and flux along the endosomal pathway, which in turn modulates cellular lipid homeostasis. These results underscore the importance of endosome functions for LD formation and reveal a previously unknown regulatory mechanism of the cellular programs controlling lipid storage and endosome transport under the control of Wnt signaling.

Keywords canonical Wnt signaling; endosomes; functional genomics; LDL-derived cholesterol; lipid droplets
Subject Category Membrane & Intracellular Transport
DOI 10.15252/embr.201540081 | Received 12 January 2015 | Revised 5 March 2015 | Accepted 6 March 2015 | Published online 7 April 2015
EMBO Reports (2015) 16: 741–752

Introduction

There is growing appreciation for the diverse and fundamental role of lipids and lipid metabolism in cell biology [1,2]. Beyond their important functions as storehouses of energy for the cell and in establishing membrane physical behavior, lipids are now recognized as regulators of protein function and as important second messengers. Cholesterol, the chief sterol of mammalian cells, functions in all of these roles and is central to lipid homeostasis [3].

Most mammalian cells can synthesize cholesterol *de novo*, but they primarily acquire cholesterol via endocytosis of low-density lipoprotein (LDL) by the LDL receptor (LDLR) [4]. Internalized LDLs are transported to late endosomes where esterified cholesterol is then released and de-esterified. This free cholesterol is exported to the endoplasmic reticulum (ER) and on to the rest of the cell [4,5]. In the ER, cholesterol can be re-esterified into cholesteryl esters (CEs) and stored with triacylglycerides (TAGs) in lipid droplets (LDs)—discrete organelles that function as a repository to supply the future lipid needs of the cell [6].

The Wnt pathway is well understood as a determinant of developmental expression and differentiation and has a causative role in several human diseases of the connective tissue and bones and in cancer [7]. The Wnt proteins themselves are typically lipid-modified and are secreted by the cells where they serve as both long- and short-range ligands for various receptors and co-receptors, the best characterized of which are the frizzled family of receptors [7,8]. In the canonical Wnt pathway, frizzled activation leads to destabilization of the adenomatous polyposis coli (APC) complex, and the stabilization of factors that translocate to the nucleus and interact with the TCF/LEF family of transcription factors to regulate gene expression [7].

The Wnt pathway may also influence lipid storage. In mice, a liver-specific knockout of β-catenin results in both steatosis (the excessive accumulation of cellular lipids) and a marked increase of cholesterol levels in the liver [9]. Furthermore in mice, LRP1 (low-density lipoprotein receptor-related protein 1) ablation may direct adipocyte differentiation and intracellular cholesterol accumulation through the Wnt pathway [10].

Herein, we used high-content genome-wide RNAi screens and found with this unbiased strategy that Wnt3a regulates cellular cholesterol. We now show that Wnt3a stimulation potentiates the production of cellular LDs that are dependent on LDL-derived cholesterol. Moreover, these dramatic changes in cellular lipid homeostasis are effected by the modulation of the endocytic pathway via the canonical Wnt pathway. These results underscore

1 Department of Biochemistry, University of Geneva, Geneva, Switzerland
2 Faculty of Sciences, Institute of Molecular Life Sciences, University of Zurich, Zurich, Switzerland
3 Vital-IT Group, Swiss Institute of Bioinformatics, University of Lausanne, Lausanne, Switzerland
4 Biomolecular Screening Facility, SV-PTECH-PTCB, Swiss Federal Institute of Technology (EPFL), Lausanne, Switzerland
*Corresponding author. Tel: +41 22 379 3464; E-mail: jean.gruenberg@unige.ch
†Present address: CeMM Research Center for Molecular Medicine, Vienna, Austria

the importance of the endosome function for LD formation and reveal a previously unknown mechanism of regulation of the LD cellular program under the control of Wnt signaling.

Results

Functional genomics and high-content screening for genes regulating cholesterol

We undertook an image-based, genome-wide siRNA screens for genes that influence cholesterol, using the cholesterol-binding compound filipin which conveniently emits in the UV range (Fig 1A–C). Since LDL-cholesterol is de-esterified in the late endosomes (see Fig 1D), where it accumulates in the cholesterol storage disorder Niemann–Pick type C (NPC) [5,11], we chose to simultaneously detect the late endosomal lipid lysobisphosphatidic acid (LBPA) with the monoclonal antibody 6C4 [12]. LBPA is not detected elsewhere in the cells and is intimately linked to cholesterol, since interfering with its functions phenocopies NPC at the cellular level [12,13].

Using filipin and the anti-LBPA antibody, we established a robust imaging assay (Fig 1C) and screened two human cell lines selected for their amenability for imaging, HeLa-MZ and A431, an epithelial tumor cell line known to contain an abundant endocytic pathway (Fig 1B). Images were acquired by an automated microscope, processed by segmentation and analysis algorithms, and candidate genes were then further refined by population context correction [14]. The assay was validated by calculating the *z*-score of non-targeting siRNAs, as negative controls, versus our positive control after NPC1 depletion with siRNAs (*z*-score > 0.5), using machine learning algorithms. Indeed, LDL-derived cholesterol increased after knockdown of NPC1 and decreased after LDL receptor (LDLR) depletion (Fig 1C). This analysis revealed that the amounts of LBPA and cholesterol were globally correlated over the screen (Fig 1E), as also revealed after NPC1 knockdown (Fig 1C). Multidimensional analysis also revealed that many of the genes annotated as present in the canonical Wnt pathway formed a group, divergent from the bulk of the cells imaged in the screen (Supplementary Fig S1A). Indeed, pathways analysis showed that the Wnt pathway genes were highly enriched in our screens ($P = 5.93 \times 10^{-4}$; Supplementary Fig S1B).

The Wnt pathway as a regulator of cellular cholesterol homeostasis

Since Wnt ligands are lipidated and difficult to purify [8], we prepared conditioned media from Wnt3a-expressing L cells [15]. When added to naïve HeLa-MZ and L cells, the conditioned media strongly stimulated the Wnt pathway as assessed by β-catenin accumulation (Supplementary Fig S2A) and increased nuclear localization (Supplementary Fig S2B)—as expected from activation of the Wnt signaling pathway [7]. Unless indicated, L cells were used in subsequent experiments, because of lower background activation (Supplementary Fig S2A). As expected from the screen, Wnt3a decreased free (membrane) cholesterol by ~20% after 24 h (Fig 2A–C; Supplementary Fig S2C and D)—a highly significant decrease, since cells tightly regulate membrane cholesterol levels [16]. Knockdown of APC recapitulated the observed decrease in membrane cholesterol (Fig 2B and C), confirming the specificity of Wnt3a effects on membrane cholesterol. Interestingly, concomitant with the reduction in membrane cholesterol (Fig 2A–C), Wnt3a profoundly increased the amount of cholesteryl esters (CEs) (Fig 2D), and the incorporation of [^{3}H]-oleic acid into CEs and triacylglyceride TAGs (Fig 2E; Supplementary Fig S3C).

Wnt3a stimulation induces lipid droplet formation

As the primary storage site of CEs and TAGs in cells is lipid droplets (LDs), we next examined the protein levels of the lipid droplet coat protein PLIN2 (Supplementary Fig S3B) and found they were greatly increased by Wnt3a, as were the mRNA levels of the TAG lipase PNPLA2 (Fig 2K right; Supplementary Fig S3A), and of SOAT1 (Fig 2K left) and DGAT2 (Fig 2K middle), which produce CEs [17] and TAGs [18], respectively. While very few, if any, LDs were seen in controls (Fig 2F; left inset), Wnt3a greatly increased the number of LDs (Fig 2F; right inset), ≈40-fold at 48 h post-stimulation (Fig 2F). Much like it did on free cholesterol levels (Fig 2B and C), APC knockdown fully recapitulated Wnt3a effects on LD formation (Fig 2G), confirming the role of the Wnt pathway. Similarly, Wnt3a-induced LD formation was prevented by recombinant DKK1 (Fig 2H), a potent extracellular inhibitor of Wnt signaling [19]. Finally, treatment of control cells with 100 μg/ml oleic acid (Supplementary Fig S3D) stimulated LD formation as expected [6,20]. Nevertheless, Wnt3a, when added to oleic acid-treated cells, further increased the size and number of LDs in a very dramatic manner (Fig 2I and J). Hence, Wnt3a stimulates massive droplet formation, when fatty acids are not limiting. Altogether, our data demonstrate that Wnt3a induces LD formation via the canonical Wnt pathway.

As the liver is central to cholesterol and lipid homeostasis in the organism, we next sought to check whether Wnt3a induced lipid droplets in a liver model. To this end, we treated the terminally differentiated HepaRG hepatocyte cell model [21,22]

Figure 1. High-content screens for modulators of intracellular cholesterol homeostasis.

A Summary of image-based screening assay for modulators of endosomal cholesterol and LBPA.

B Schema outlining cell types, libraries and strategies used for screening and analysis.

C Representative images from the screen including merged image with segmentation (top panels), the filipin (free cholesterol) channel (middle panels) and the anti-LBPA antibody stain (bottom panels) are shown for the control, as well as the knockdown of NPC1 and LDLR.

D Representation of cellular trafficking pathways relevant in LDLR-mediated cholesterol influx. Indicated are LDLR (green) and LDL particles and LDL-derived cholesterol (blue) and LBPA-containing membranes (red). LBPA is abundant in the intralumenal membranes of late endosomes [13].

E Example of one of the correlations summarized in (F), presented as a density plot of the mean cholesterol signal versus mean LBPA signal for each gene tested overlaid with a linear regression trend line (red). Data are from the HeLa-MZ, library 2 screen and are the means of two replicates of the screen for each siRNA pool.

F Pathways most enriched in the siRNA screens. Node size is indicative of the number of genes present in each pathway, while node color represents the statistical significance of the enrichment.

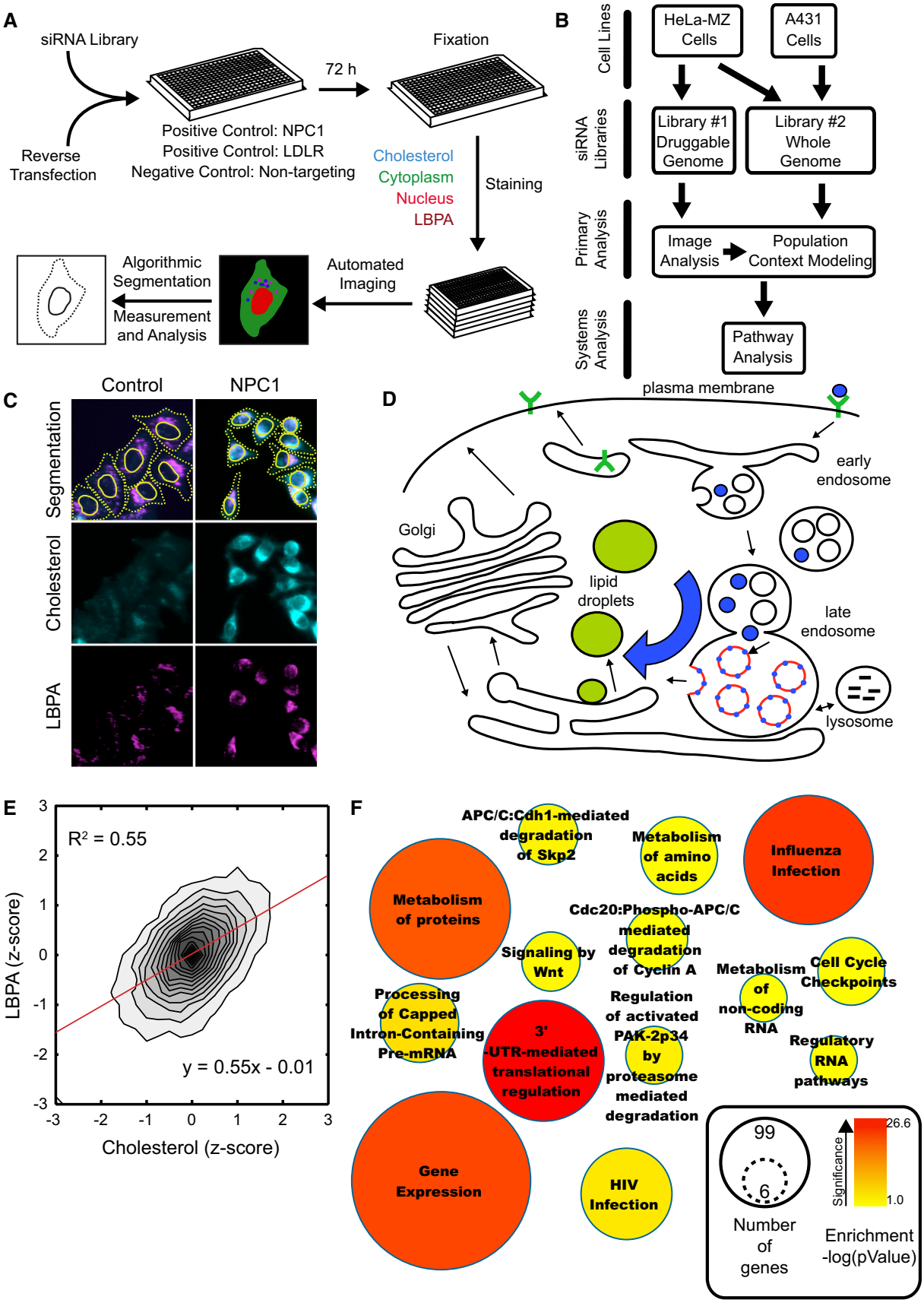

Figure 1.

with Wnt3a-conditioned media for 24 h. Like in the other cell lines we tested, Wnt3a induced a significant increase in the size (Fig 3A) and number (Fig 3B) of lipid droplets, and a concomitant increase in the cellular amounts of CEs (Fig 3C). These results, in concert with the previously described role of β-catenin in hepatic lipid regulation [9], suggest a physiological function for the Wnt pathway in the regulation of lipid metabolism by the liver.

Transcriptional analysis of the Wnt response

That the Wnt response had been elicited by Wnt3a was confirmed by a transcriptomic analysis—Wnt3a significantly changed ($P = 0.0015$) the expression of Wnt-responsive genes (Supplementary Fig S4; Supplementary Table S1; see also the analysis of the Wnt-induced transcriptional response in the Supplementary Information). This analysis also showed that Wnt

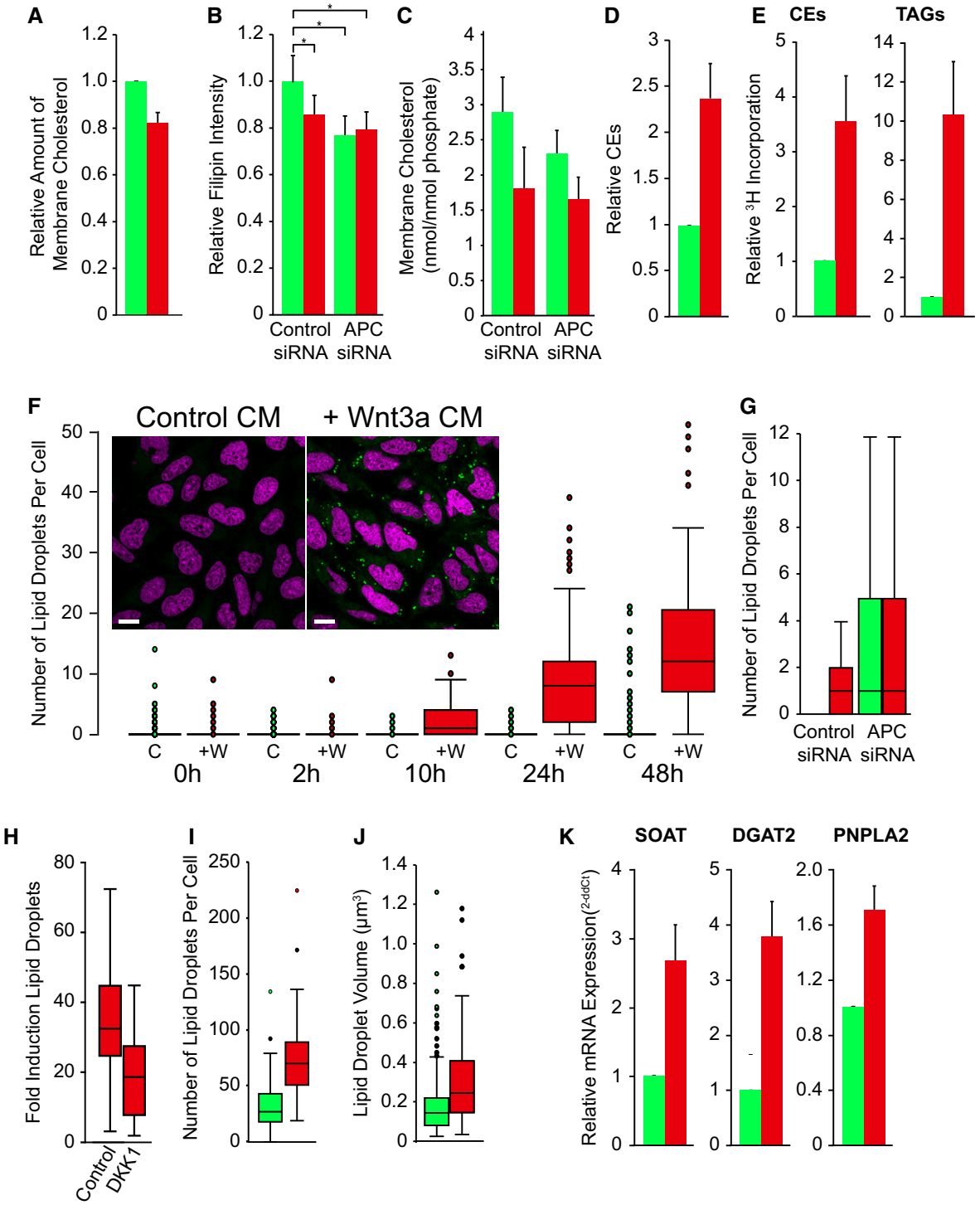

Figure 2.

Figure 2. Effect of Wnt3a addition on membrane cholesterol, CEs and LDs.

A HeLa-MZ were cultured with control- (green bars) or Wnt3a-conditioned media (red bars) for 24 h, before lipid extraction and quantitation by GC-MS; free cholesterol was quantified (mean ± SEM) from integration of the resulting peaks. $N = 3$.

B, C HeLa-MZ (B) and L cells (C) were treated as in (A) for 24 h after transfection with non-targeting (AllStar) or anti-APC siRNAs; the filipin intensity of the micrographs (an average of 450 cells per condition) (B) and free cholesterol (mean and standard deviation of a representative of two independent experiments analyzing at least 2,500 cells) (C, quantified as in A) were analyzed. * indicates a *P*-value approaching 0 (Student's *t*-test).

D L cells were treated as in (A), except that CEs were quantified after 24 h. Mean ± SEM; $N = 6$; $P = 0.07$.

E L cells treated as in (A) for 24 h were co-incubated in the presence of ^{3}H-oleic acid; CEs and TAGs were extracted and analyzed by thin-layer chromatography. Mean ± SEM; $N = 5$; $P = 0.016$ (CEs) and 0.027 (TAGs).

F L cells treated as in (A) were fixed, stained with BODIPY 493/503 (green) to label LDs and DAPI (magenta) and imaged by confocal microscopy (inset; scale bars: 10 μm). Quantitation of LDs after Wnt3a addition is presented as a boxplot as indicated. Data are the combined distribution of three independent experiments.

G Cells treated with control or anti-APC siRNAs for 48 h before Wnt3a addition (A) were stained with BODIPY 493/503 and LDs quantified. Representative distribution (boxplot) of at least 4,000 cells per condition from three independent experiments.

H Cells were treated as in (A), in the absence (control) or presence of recombinant mouse DKK1 and a boxplot of the LDs per cell is presented for over 25 fields; $P = 0.014$.

I, J Cells treated as in (A) in the presence of 100 μg/ml oleic acid to induce LD formation were fixed and stained with BODIPY 493/503 and the volume (J) and number (I) of LDs quantified; $P = 3 \times 10^{-5}$ (I, LD number) and 6×10^{-6} (J, LD volume). Data are presented as a representative boxplot of two independent experiments where at least 30 cells were counted per experiment.

K L cells treated as in (A) were incubated as indicated and analyzed by qRT–PCR; data represent ddCt values as a fraction (mean ± SD) of the control. $N = 3$.

Data information: Green bars, control CM; red bars, Wnt3a CM.

regulates sterol ($P = 2.3 \times 10^{-6}$) and lipid ($P = 5.0 \times 10^{-8}$) metabolism at the transcriptional level (Supplementary Fig S4C). Furthermore, the top 101 genes upregulated upon treatment with U18666A, a drug that mimics the cholesterol storage disorder Niemann–Pick type C (NPC) [5], overlapped highly significantly (47 genes; $P = 0$; Supplementary Fig S5A and Supplementary Table S2) with Wnt-responsive transcripts. In sum, these data establish the role of the Wnt pathway in the regulation of lipid metabolism at the cellular level. The two treatments affected cholesterol-related gene expression in opposite directions. U18666A increased the expression of cholesterol-related genes, presumably because the drug, by mimicking NPC [23], uncouples cholesterol uptake from the SREBP-dependent regulation of cholesterol accumulation [5]. By contrast, Wnt3a-treatment reduced the amounts of mRNA detected, suggesting that cholesterol does not originate from biosynthetic sources during LD biogenesis.

Wnt3a-induced changes in lipid homeostasis are dependent on the flux of cholesterol through the endosome

To address the source of cholesterol in Wnt3a-induced LDs, we incubated cells with Wnt3a in lipoprotein-depleted serum (LPDS) (Fig 4A) or after LDLR silencing (Fig 4B) and found that such treatments completely abolished CE accumulation and dramatically reduced the number of LDs—LDs, however, were still detected (Supplementary Fig S3E). Indeed, incubation in LPDS ablated Wnt3a-induced cholesterol esterification (Fig 4C, left), but did not affect TAG esterification (Fig 4C, right; see the analysis of Wnt-dependent regulation of LD formation: CEs and TAGs in the Supplementary Information). Next, we found that the Wnt3a-induced LD biogenesis was diminished when early-to-late endosome transport was inhibited (Fig 4D) by overexpression of the active Q79L mutant of the small GTPase Rab5 [24]. Similarly, Wnt3a-induced LD biogenesis was also inhibited by endocytosed anti-LBPA antibodies (Fig 4E), which inhibit cholesterol export from late endosomes and phenocopy NPC [25,26]. In late endosomes, LIPA normally converts LDL-derived CE to free cholesterol [27] (Fig 1D). The general lipase inhibitor orlistat, which targets LIPA, caused CE accumulation (Fig 4F), but inhibited the neo-synthesis of ^{14}C-labeled CEs after metabolic labeling (Fig 4G). This demonstrates that LDL-derived CE is the source of cholesterol for re-esterification by SOAT and incorporation into Wnt-induced LDs. Indeed, the specific SOAT inhibitor 58-035 [28] completely blocked CE accumulation in response to Wnt (Fig 4F and G). Hence, the cholesterol flux through—and export from—endosomes is required to support the full-scale Wnt response for fueling LD biosynthesis.

Wnt and endocytosis: regulation of cholesterol transport gene expression

One might have expected LDLR expression to be increased via the SREBP pathway [4] when membrane cholesterol decreases in response to Wnt3a. However, Wnt3a decreased LDLR mRNA (Fig 5C) and protein (Fig 5D), as well as LDL cell surface binding (Fig 5A). Again, much like membrane cholesterol levels and LD number, these effects of Wnt were mimicked by APC knockdown (Fig 5B). Wnt3A also decreased both the mRNA (Fig 5E) and protein (Fig 5F) levels of NPC2, which is responsible when mutated for the NPC disorder [5]. However, no significant change was observed in the transferrin receptor, the early endosome marker EEA1, and the late endosome markers Rab7 and LAMP1 (Supplementary Fig S6A), or in the acidification properties of endosomes and lysosomes (Supplementary Fig S6C) and the kinetics of EGF receptor degradation after EGF challenge (Supplementary Fig S6B). Wnt3a slightly reduced initial fluid-phase uptake (Supplementary Fig S6D and E), likely reflecting the role of cholesterol in L cell endocytosis [29]. Hence, Wnt3a does not cause global alteration of endosomal membrane composition and dynamics, but induces specific changes in the cholesterol transport machinery.

The sterol regulatory element-binding proteins (SREBPs) are central transcriptional regulators of the cholesterol metabolism and lipogenesis through driving expression of many genes, including LDLR [30]. Consistent with this notion, we found that Wnt3a treatment potently reduced the expression of both SREBP1 (Fig 5H) and SREBP2 (Fig 5I). Since Wnt3a stimulates cholesterol storage and

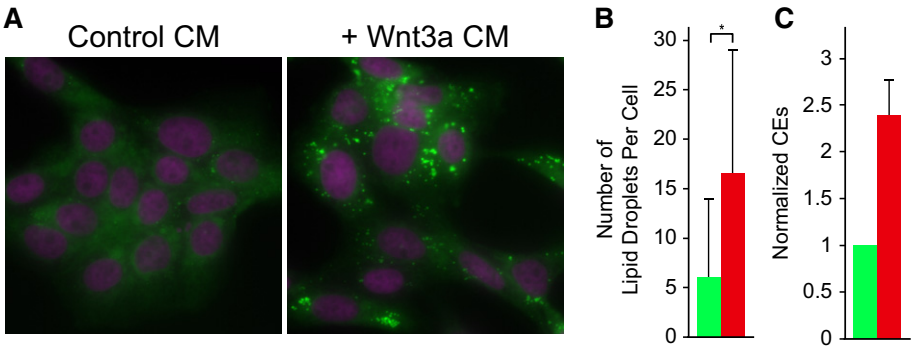

Figure 3. Effect of Wnt3a on LD in HepaRG cells.

A Differentiated HepaRG cells were treated with control- or Wnt3a-conditioned media for 24 h before fixation and LD quantitation as in Fig 2F.

B Representative distribution of the mean ± SD of (A) from three independent experiments where at least 10,000 cells were counted. * indicates a *P*-value approaching 0 (Student's *t*-test). Green bars, control CM; red bars, Wnt3a CM.

C HepaRG were prepared as in (A), and the amount of CEs was determined as in Fig 2D. Data are the mean ± SEM of six independent experiments. Green bars, control CM; red bars, Wnt3a CM.

decreases uptake, it may activate a cholesterol preservation mode via feedback loops that positively and negatively regulate biosynthesis and uptake, respectively.

The Wnt response and viral infection

Recently, vesicular stomatitis virus (VSV) was shown to use LDLR family members as cell surface receptors [31]. Strikingly VSV infection was markedly (~50%) reduced by Wnt3a (Fig 5G), but to our initial surprise, LDLR knockdown had no effect on VSV binding to the cell surface (Supplementary Fig S6F), infection and Wnt3A response (Supplementary Fig S6G). However, VSV infection could be increased by LDLR overexpression, in a process that remained fully Wnt3a dependent (Supplementary Fig S6H). We thus conclude that, when LDLR is reduced, VSV infection is supported by other LDLR family members, as expected [31]. Previous studies showed that infection with VSV [13,32,33] and old world arenaviruses [34] as well as intoxication with anthrax [35,36] depends on the late endosomal lipid LBPA. Since interfering with LBPA functions phenocopies the cholesterol storage disease NPC [25,26] and inhibits the Wnt-induced LD accumulation (Fig 4E), it is attractive to believe that Wnt3a affects the endosomal pathway at a distal step, from where viral capsids and cholesterol are exported.

Discussion

Our data underscore the importance of cholesterol storage in cellular lipid homeostasis and demonstrate that Wnt-induced cholesterol storage in LDs requires LDLR-mediated endocytosis, trafficking of incoming CEs along the endocytic pathway, de-esterification by LIPA, export from the late endosomes to the ER and re-esterification by SOAT. We thus conclude that Wnt3a stimulates the flux of endocytosed, LDL-derived cholesterol toward LDs, where it accumulates as CEs. At first glance, however, it may seem at odds that Wnt3a promotes both the inception of LDs and the concomitant storage of lipids in the form of CEs and TAGs, while eventually decreases the flux of incoming material through the endocytic pathway. However, cholesterol homeostasis is tightly regulated and cells likely respond to the flux of lipids into LDs by reducing LDL-derived cholesterol availability through the SREBP-mediated sterol response pathway [4]—and indeed the expression of cholesterol-regulated genes is decreased by Wnt including SREBPs themselves. Down-regulation of the LDLR and of endosomal transport in general, by reducing the rate of incoming material, protects cells from the deleterious effects of an overabundance of intracellular lipids.

Much like the Wnt response [7,8], an increase in LDs has been correlated with human cancer progression [37], and a causal link was found between LD density and the proliferation of colonic epithelia cells [38]. Moreover, overexpression of genes regulating endocytic uptake of lipids have been linked to the invasiveness of metastatic cancers [39], and more directly, the proliferation of nasopharyngeal carcinoma cells has been show to depend on LDL [40]. We thus speculate that the ability of Wnt to induce LD accumulation is linked with its oncogenic activity: Wnt-dependent regulation of LDs may serve to exert pro-proliferative effects, both in developmental and in pathological contexts. Hence, inhibitors of LD formation or cholesterol flux may provide candidate drugs for the treatment of cancers, especially Wnt-driven tumors. We conclude that, since Wnt-induced LD formation is controlled by and controls endosomal functions, a tight feedback regulation exists between the Wnt response, endosome trafficking and lipid flux within endosomes.

Materials and Methods

Cells, media, reagents and antibodies

HeLa-MZ cells, provided by Marino Zerial (MPI-CBG, Dresden), and Epithelial A431 cells [41] were selected to be amicable to imaging. L cells (ATCC: CRL-2648) and L Wnt3a cells (ATCC: CRL-2647) were provided by Gisou van der Goot (École Polytechnique Fédérale de Lausanne). HepaRG cells were provided by Ueli Schibler (University of Geneva) and are described previously [21,22]. As Wnt ligands

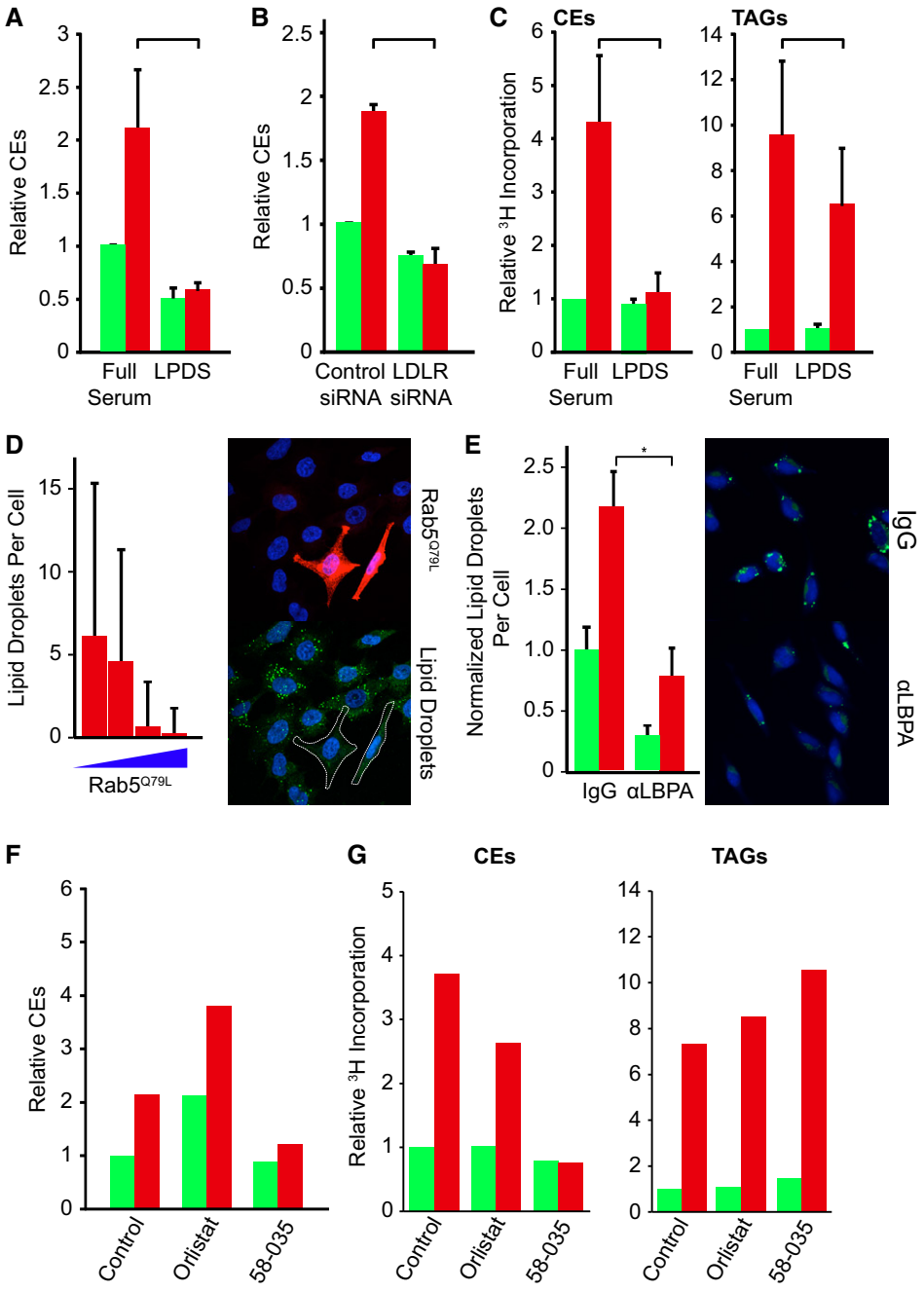

Figure 4. Wnt3a-induced LD dependence on LDLR and endosomal factors.

A CEs from L cells were treated as in Fig 2A but using conditioned media prepared using lipoprotein-depleted serum (LPDS) or full serum for 24 h, were extracted and were quantified by GC-MS. $N = 4$, $P = 0.04$.

B Cells were pre-treated with control or anti-LDLR siRNAs for 48 h and then treated and analyzed as in Fig 2A, before CE quantification as in (A). Data are the mean ± SD of a representative of two independent experiments; $P = 0.02$.

C Lipids were extracted from L cells treated as in Fig 2A in the presence of ^{3}H-oleate and quantified by TLC for CEs (left) or TAGs (right). $N = 3$; $P = 0.032$ (CEs) and 0.039 (TAGs).

D HeLa-MZ cells pre-transfected with Rab5^{Q79L}-mCherry were treated as in Fig 2A, fixed, stained for LDs and imaged. Data are presented as the mean ± SD of the number of LDs per cell binned according to Rab5^{Q79L}-mCherry expression (see Materials and Methods).

E L cells were treated as in Fig 2A in the presence of 10 μg/ml anti-LBPA or control IgGs and analyzed by light microscopy after LD staining and quantification as in Fig 2F. Data are presented as the mean ± SD of at least 3,500 cells per condition. * indicates a P-value approaching 0 (Student's t-test).

F, G Cells were incubated for 16 h with orlistat (5 μM) or Sandoz 58-035 (10 μM). Lipids were extracted and quantified as above by GC-MS (F) or TLC (G). Data are the mean of 2 (58-035) or 3 (orlistat) independent experiments.

Data information: Green bars, control CM; red bars, Wnt3a CM. Data are presented as the mean ± SEM of indicated number of independent experiments unless otherwise indicated.

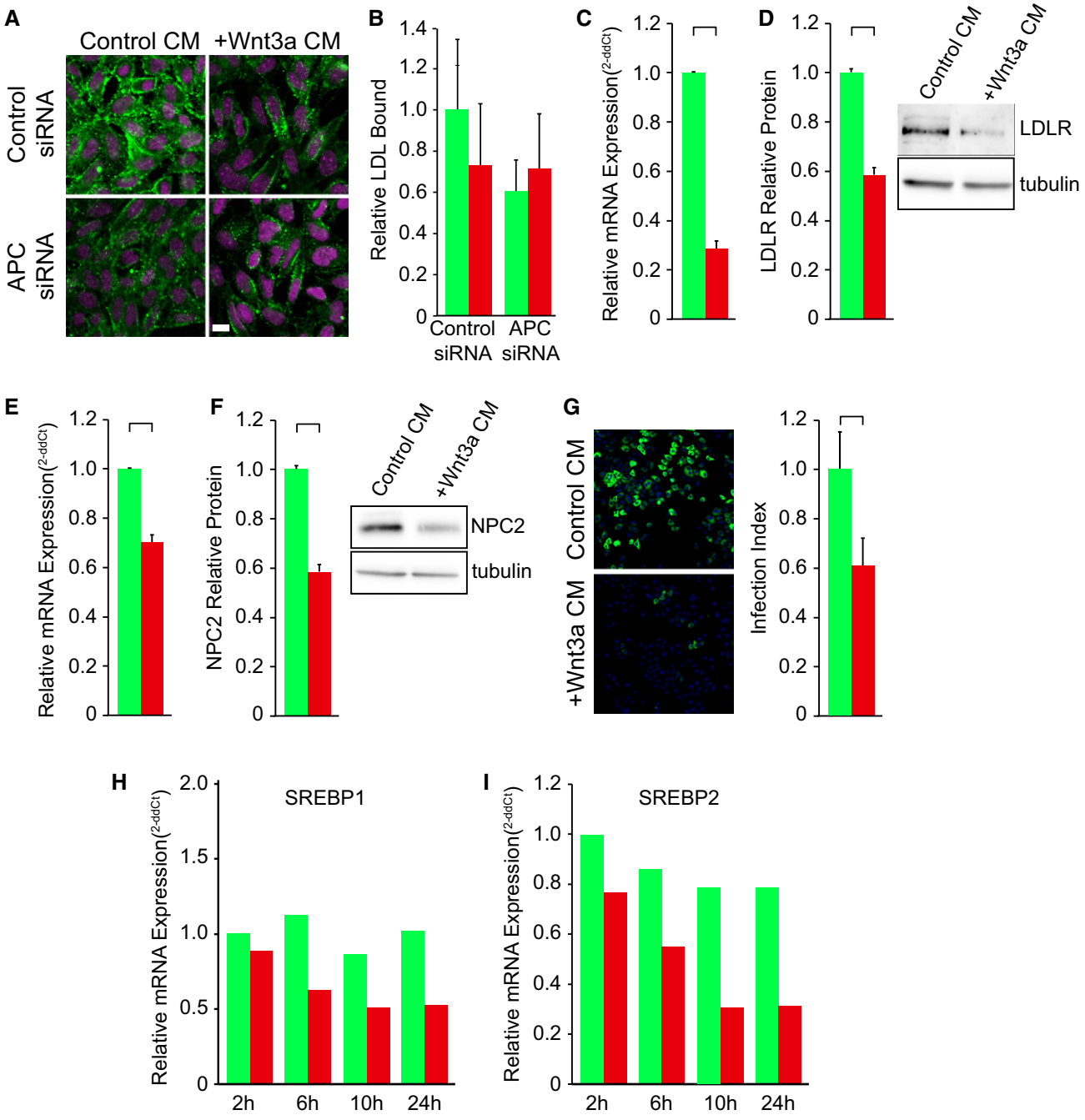

Figure 5. Effect of Wnt3a on the cholesterol influx pathway.

A, B Cells pre-incubated with control or anti-APC siRNAs for 24 h were further incubated with fluorescently labeled LDL in conditioned media on ice. The cellular intensity of LDL was quantified (B) and is shown relative to the control (right). Representative mean ± SD of at least 750 cells.

C, D L cells treated as in Fig 2A were analyzed by qRT–PCR for LDLR mRNA (C) or by Western blotting with antibodies to LDLR (D). In (C), data are represented as ddCt values and are the means ± SEM of four independent experiments; $P = 0.01$. In (D), quantification of the blots is shown as the means ± SEM of five independent experiments (representative blot shown in the inset); $P = 0.03$.

E, F The experiment and analysis were as in (C, D) except that NPC2 mRNA ($N = 3$) (E) and protein ($N = 3$) (F) levels were analyzed (mean ± SEM); $P = 1 \times 10^{-5}$ (E) and $P = 6 \times 10^{-4}$ (F).

G HeLa-MZ cells pre-treated as in Fig 2A were incubated on ice with 1 MOI VSV expressing GFP-tagged P protein (L cells are refractory to VSV infection) and, then at 37°C for 2.5 h, fixed and imaged. Cells were scored as infected by the presence of the VSV-P-GFP protein by automated image analysis. Data are the mean ± SD of at least 18 individual fields of cells (20× magnification) scored; $P = 2 \times 10^{-8}$.

H, I L cells were treated as in (C) for the indicated times but with primers to SREBP1 (H) and SREBP2 (I). Data are represented as ddCt values and are the means of two independent experiments.

Data information: Green bars, control CM; red bars, Wnt3a CM.

are lipidated and thus difficult to purify [8], we prepared Wnt3a-conditioned media from Wnt3a-expressing L cells as a source of ligand—a well-established approach to study Wnt signaling [15]—and control-conditioned media from control L cells. VSV-PeGFP was provided by Asit Pattnaik (University of Nebraska-Lincoln). Reagents were sourced as follows: oligonucleotides and small interfering RNA (siRNA) from Qiagen (Hilden, Germany) or Dharmacon (Lafayette, CO); DAPI, BODIPY 493/503, 5-chloromethylfluorescein diacetate (CMFDA; CellTracker Green), propidium iodide and RNase A from Invitrogen (now Life Technologies AG; Basel, Switzerland); and fluorescently labeled secondary antibodies from Jackson ImmunoResearch Laboratories (West Grove, PA). The monoclonal antibody against LBPA (6C4) has been described [12]. The anti-PLIN2 antibody (AP 125) was from Progen Biotechnik (Heidelberg, Germany), the anti-LDLR (#10007665) from Cayman Chemical Company (Tallinn, Estonia), the rabbit anti-NPC2 (HPA835) from Sigma-Aldrich (St. Louis, MO) and anti-PNPLA2 (#2138) from Cell Signaling Technology, Inc. (Danvers, MA). [9,10-^{3}H] oleic acid (45 Ci/mmol) was from PerkinElmer, Inc. (Waltham MA). Other chemicals and reagents were obtained from Sigma-Aldrich.

Transfections of cDNA were performed using Fugene 6 (Roche; Basel, Switzerland) for HeLa-MZ cells and Lipofectamine LTX (Life Technologies AG; Basel, Switzerland) for L cells using the supplier's instructions. Transfections of siRNA were accomplished with Lipofectamine RNAiMax (Life Technologies AG; Basel, Switzerland) using the manufacturer's instructions.

High-content screening

Genes influencing cellular cholesterol and LBPA were systematically screened using a four-color imaging assay relying on propidium iodide (nucleus) and CMFDA (CellTracker Green; cytoplasm) for cell segmentation, filipin III to label cholesterol and the anti-LBPA antibody, followed by CY5 anti-mouse secondary antibodies. HeLa-MZ cells were screened against a druggable genome library (three individual siRNAs; Human Druggable Genome siRNA Set v2.0 from Qiagen, Hilden, Germany) and a Dharmacon whole-genome library (three pooled siRNAs; Human Genome ON-TARGET plus SMART pool siRNA library (G-105005-E2) from Thermo Fisher Scientific, Waltham, MA), while A431 cells were screened with the Dharmacon library alone. Images were collected on a BD Pathway 435 (Becton, Dickinson and Co.; Franklin Lakes, NJ) automated microscope and processed using automated segmentation and quantitation using CellProfiler [42] software. All libraries were screened in duplicate. As quality control for the plates, we used the following: (i) a phenotypic (machine learning) step where the Z' factor for each plate was calculated using the control wells and $Z' < 0.5$ were excluded and (ii) the correlation of LBPA and cholesterol intensities across the wells of replicate plates was determined; outliers were rejected and the plate repeated.

Candidate genes were corrected for the influence of population context as described [14]. Briefly, in this modeling approach, the cellular population was binned into classes based on general cellular parameters (e.g. cellular size or cell density) to allow the direct comparison of parameters in cells of a similar state and environment, thus reducing the influence of indirect changes in population context induced by each siRNA. For pathway analysis, all data points for each gene in each screen were averaged (6 data points for Library 1–3 siRNAs in duplicate, two data points for Library 2–1 pooled siRNA of three siRNAs in duplicate) after filtering for low cell number and z normalization per plate. Hits from each screen were determined defining a hit as genes with a z-score > 1.7–2.2 and then combined into one dataset for further analysis. Enrichment in various biological pathways was determined using the Database for Annotation, Visualization and Integrated Discovery (DAVID) annotation enrichment Web service v6.7 [43] and the Reactome pathway database [44,45].

Fluorescent light microscopy

Cells were fixed in 3% paraformaldehyde for 20 min before treatment with filipin (50 μg/ml), RNase (200 μg/ml) followed by propidium iodide (5 μg/ml), BODIPY-493/503 (1:1,000; 1 mg/ml in ethanol stock) and anti-PLIN2 or anti-LBPA antibodies followed by CY5 anti-mouse secondary antibodies (1:500; 1.5 mg/ml stock). The intrinsic ability of filipin was used to permeabilize cells where present [25], but when necessary, a 10-min treatment of 0.1% saponin in PBS was used instead. Cells were either mounted in Mowiol 4-88 mounting medium (Life Technologies AG; Basel, Switzerland) and imaged with a Zeiss 700 confocal microscope (Carl Zeiss AG; Oberkochen, Germany) using a 63× objective or were left in PBS and imaged in multi-well imaging plates (BD Falco; cat# 353219) by an ImageXpress Micro XL automated microscope (Molecular Devices LLC; Sunnyvale, CA) using a 60× air objective. When necessary, nuclei were stained with 5 μg/ml DAPI in the mounting medium or in PBS. For the Rab5^{Q79L} experiments, cells were transiently transfected with a mCherry-tagged version of the mutant and expression levels were separated into four bins based on cellular mCherry intensity overall range, and the average number of lipid droplets per cell in each bin determined (22–300 cells per bin). The LBPA antibody uptake experiments were as described [12]. When appropriate, images were quantified using CellProfiler [42]. Briefly, LDs were quantified by filtering the image using the enhance speckle module set for objects of lipid droplet size, and the filtered image was processed using the standard object identification module of CellProfiler. LD size was estimated inferring the volume of a sphere from the manually measured diameter of the BODIPY 493/503 signal [20].

Gas chromatography mass spectrometry

Cells were grown to near confluence on 6-cm plastic plates before washing with, and then scraped into, cold PBS followed by centrifugation for 5 min at 300 g at 4°C. Cell pellets were resuspended in 100 μl cold water before addition of 360 μl methanol and the internal standard ergosterol (20 nmol). Next, 1.2 ml of 2-methoxy-2-methylpropane (MTBE) was added and the samples vortexed at 4°C for 10 min followed by 1 h shaking at room temperature to allow complete lipid partitioning. A total of 200 μl of water was added to induce phase separation, and the upper phase was collected and dried. On the day of reading, samples were resuspended in chloroform/methanol (1:1), sonicated for 5 min and diluted (1:2) with the same solvent. They were flushed with nitrogen gas and run on a Varian 320 ms gas chromatography mass spectrometer (Agilent Technologies; Santa Clara, CA). Membrane cholesterol and cholesteryl ester amounts were normalized and

calibrated using the total phosphate content and the integrated signal of a spiked ergosterol standard.

Cellular experiments

A recombinant vesicular stomatitis virus (VSV-PeGFP) [33,46] was used to infect cells seeded in 96-well imaging plates as described [32,33]. After staining cells with DAPI, VSV binding or infection was quantified by CellProfiler and machine learning with CellProfiler Analyst [42,47]. To study fluid-phase endocytosis, cells were incubated with 10 mg/ml Texas Red Dextran for the indicted times [48]. The nuclei were stained with DAPI (0.5 μg/ml), and fluorescence was measured by automated microscopy, using cells not exposed to dextran as background, which was subtracted from the values. Alternatively, cells were incubated with 2 mg/ml of HRP, a post-nuclear supernatant was prepared and HRP was quantified biochemically [49]. To study LDL binding to the plasma membrane, cells were seeded on coverslips or in 96-well plates for 6 h, and then, the medium was replaced with control-conditioned or Wnt3a-conditioned media, and cells were further incubated for 24 h. After washing three times with PBS, cells were incubated with 5 μg/ml DiI-labeled human LDL (Life Technologies AG; Basel, Switzerland) in HEPES-buffered (10 mM; pH 7.4) GMEM for 1 h at 4°C. Cells were washed three times with PBS, fixed with PFA and counterstained with DAPI for microscopy.

Pathway analysis of existing datasets

Gene expression array datasets from the Gene Expression Omnibus (GEO; [50]) were analyzed for Wnt3a-perturbed genes using the GEO2R online tool (http://www.ncbi.nlm.nih.gov/geo/geo2r/), an implementation of the GEOquery and limma packages from the Bioconductor project [51,52]. Genes significantly different between the control and Wnt3a-treated conditions ($P < 0.05$) were taken and compared to the indicated ontology categories and compared with a hypergeometric distribution to determine the significance of the observed pathway enrichment. Previously described Wnt3a datasets used included OP9 murine stromal cells (GSE30791), CHRF288-11 human megakaryocytes (GSE42071), C57MH murine mammary epithelial cells (GSE32096), HeLa human cells, G1 phase (GSE50248) and B16 murine melanoma cells (M-TAB-3012).

Sample preparation for microarray analysis

HeLa-MZ cells were seeded for 5 h before addition of control- or Wnt3a-conditioned media for 24 h before direct lysis into RNeasy Lysis Buffer (Qiagen). Both conditions were assayed in independent biological triplicates, and cells were prepared in parallel for BODIPY staining to confirm the presence of the LD phenotype as a control for activity of the media. Purification of total RNA was done with the RNeasy Mini Kit from Qiagen according to the manufacturer's instructions. The concentration, purity and integrity of the RNA were measured with the Picodrop Microliter UV-Vis Spectrophotometer (Picodrop) and the Agilent 2100 Bioanalyzer (Agilent Technologies), together with the RNA 6000 Series II Nano Kit (Agilent) according to the manufacturer's instructions.

We used the Human Gene 2.0 ST Array Reagent kit (Affymetrix) for microarray target amplification and the GeneChip Whole Transcript Sense Target Labeling Assay (Affymetrix) for labeling. Target preparation as well as hybridization, washing and scanning was performed according to the manufacturer's instructions, as described. In general, all samples were processed simultaneously except for cleanup steps and the hybridization till scanning procedure. Sample preparation was according to the 100 ng Total RNA Labeling Protocol. Differing from the protocol, we used 200 ng of total RNA as starting material for the first-strand cDNA synthesis. The raw microarray data files were generated with the Affymetrix GeneChip Operating Software. Normalization [according to the RMA (robust multiarray averaging) procedure] [53] was done with Partek Genomics Suite v6.5. The Wnt3a microarray data are available in the ArrayExpress database (www.ebi.ac.uk/arrayexpress) under accession number E-MTAB-2872. The U18666a gene array analysis was as described [20].

Gene array pathway analysis

Normalized microarray data were analyzed for pathway representation by testing for statistical enrichment of Gene Ontology (GO) biological process. The dataset of gene with expression significant perturbed ($P < 0.01$) by Wnt3a-treatment was collected and tested using V1: GeneGo (MetaCore from Thomson Reuters; V6.16) and V2: DAVID (Database for Annotation, Visualization and Integrated Discovery annotation enrichment Web service v6.7) [43]. In parallel, this gene list was submitted to STRING (Search Tool for the Retrieval of Interacting Genes/Proteins; V9.05) to determine known and predicted interactions in the gene set [54].

Other methods

For Western blotting, cells were lysed with RIPA buffer plus protease inhibitors (1 mM phenylmethylsulfonyl fluoride, 10 μg/ml aprotinin, 1 μM pepstatin, 10 μM leupeptin) for 20 min. The lysates were sonicated and clarified by centrifugation at 18,000 *g* for 10 min at 4°C, and aliquots of 60 μg of protein were separated by SDS–PAGE and blotted on nitrocellulose membrane. RT–PCR was carried out essentially as described [20,55], after total RNA extraction using TRIzol Reagent (Life Technologies AG; Basel, Switzerland) according to manufacturer's recommendation from monolayers of HeLa-MZ or L cells. Newly synthesized CEs and TAGs were analyzed by thin-layer chromatography after incubating L cells with [9,10-^{3}H] oleic acid (45 Ci/mmol, 10 μCi/point) in a complex with fatty acid-free BSA, for 14 h, scraped from the TLC plates and quantified by scintillation counting using a β-scintillation counter (Beckman LS6500) [20]. Unless otherwise stated, all statistical tests for significance were performed with Student's *t*-distribution with a two-tailed distribution using unequal variance test. Boxplots show the interquartile range with or without the outliers.

Data availability

Primary data

Scott CC, Schaad O, Gruenberg J (2015). Wnt directs the endosomal flux of LDL-derived cholesterol and lipid droplet homeostasis. ArrayExpress E-MTAB-2872.

Referenced data

Frank B, Ichii M, Kincade P, Iozzo RV, Garrett K (2012). A supporting environment for hematopoietic stem/progenitor cells is maintained by canonical Wnt signaling. Gene Expression Omnibus GSE30791.

Macaulay IC, Maguire P (2012). Treatment of CHRF288-11 Megakaryocytic Cells with Wnt compounds. Gene Expression Omnibus GSE42071.

Baljinnyam B, Callahan R, Rubin JS (2011). Gene expression in Rspo2 and/or Wnt3a treated C57MG mouse mammary epithelial cells. Gene Expression Omnibus GSE32096.

Berger BS, Acebron SP, Karaulanov E, Niehrs C (2014). Expression profiling of Wnt3a-treated HeLa cells in G1 and G2/M phase. Gene Expression Omnibus GSE50248.

Chen A. (2007). Activation of Wnt signaling pathways in murine B16-F1 melanoma cells. ArrayExpress M-TAB-3012.

Supplementary information for this article is available online: http://embor.embopress.org

Acknowledgements

We are grateful to Mylene Docquier, Christelle Barraclough and the Genomic Platform team (Geneva University) for the transcriptomic analysis, and to Volker Flegel and Roberto Fabretti from Vital-IT (http://www.vital-it.ch) Center for high-performance computing of the SIB Swiss Institute of Bioinformatics. Support was from the Swiss National Science Foundation, the Swiss Sinergia Program, the Polish-Swiss Research Programme (PSPB-094/2010), the NCCR in Chemical Biology and LipidX from the Swiss SystemsX.ch Initiative, evaluated by the Swiss National Science Foundation (to J. G.). C. C. S. has been supported by fellowships from the Human Frontier Science Program and the Canadian Institutes of Health Research.

Author contributions

CCS carried out most of the experiments and wrote the manuscript; SV helped with the RNAi screens and the MS analyses; FV contributed to the lipid analysis; BS and LP carried out the population context analysis of the screen data; JL analyzed EGF trafficking; OS, DK, OM and NG contributed to the bioinformatics analysis of the transcriptomic data and RNAi screens, respectively; MC and GT helped with the optimization and automation of the screens; and JG supervised the entire project and wrote the manuscript.

Conflict of interest

The authors declare that they have no conflict of interest.

References

1. Santos AX, Riezman H (2012) Yeast as a model system for studying lipid homeostasis and function. *FEBS Lett* 586: 2858 – 2867
2. Wymann MP, Schneiter R (2008) Lipid signalling in disease. *Nat Rev Mol Cell Biol* 9: 162 – 176
3. Goedeke L, Fernandez-Hernando C (2012) Regulation of cholesterol homeostasis. *Cell Mol Life Sci* 69: 915 – 930
4. Brown MS, Goldstein JL (2009) Cholesterol feedback: from Schoenheimer's bottle to Scap's MELADL. *J Lipid Res* 50(Suppl): S15 – S27
5. Ikonen E, Holtta-Vuori M (2004) Cellular pathology of Niemann-Pick type C disease. *Semin Cell Dev Biol* 15: 445 – 454
6. Pol A, Gross SP, Parton RG (2014) Review: biogenesis of the multifunctional lipid droplet: lipids, proteins, and sites. *J Cell Biol* 204: 635 – 646
7. Clevers H, Nusse R (2012) Wnt/beta-catenin signaling and disease. *Cell* 149: 1192 – 1205
8. Port F, Basler K (2010) Wnt trafficking: new insights into Wnt maturation, secretion and spreading. *Traffic* 11: 1265 – 1271
9. Behari J, Yeh TH, Krauland L, Otruba W, Cieply B, Hauth B, Apte U, Wu T, Evans R, Monga SP (2010) Liver-specific beta-catenin knockout mice exhibit defective bile acid and cholesterol homeostasis and increased susceptibility to diet-induced steatohepatitis. *Am J Pathol* 176: 744 – 753
10. Terrand J, Bruban V, Zhou L, Gong W, El Asmar Z, May P, Zurhove K, Haffner P, Philippe C, Woldt E *et al* (2009) LRP1 controls intracellular cholesterol storage and fatty acid synthesis through modulation of Wnt signaling. *J Biol Chem* 284: 381 – 388
11. Vacca F, Scott CC, Gruenberg J (2014) Endosome maturation, transport and functions. *Semin Cell Dev Biol* 9: 2 – 10
12. Kobayashi T, Stang E, Fang KS, de Moerloose P, Parton RG, Gruenberg J (1998) A lipid associated with the antiphospholipid syndrome regulates endosome structure and function. *Nature* 392: 193 – 197
13. Bissig C, Gruenberg J (2013) Lipid sorting and multivesicular endosome biogenesis. *Cold Spring Harb Perspect Biol* 5: a016816
14. Snijder B, Sacher R, Rämö P, Liberali P, Mench K, Wolfrum N, Burleigh L, Scott CC, Verheije MH, Mercer J *et al* (2012) Single-cell analysis of population context advances RNAi screening at multiple levels. *Mol Syst Biol* 8: 579
15. Shibamoto S, Higano K, Takada R, Ito F, Takeichi M, Takada S (1998) Cytoskeletal reorganization by soluble Wnt-3a protein signalling. *Genes Cells* 3: 659 – 670
16. Hannich JT, Umebayashi K, Riezman H (2011) Distribution and functions of sterols and sphingolipids. *Cold Spring Harb Perspect Biol* 3: a004762
17. Miller WL, Bose HS (2011) Early steps in steroidogenesis: intracellular cholesterol trafficking. *J Lipid Res* 52: 2111 – 2135
18. McFie PJ, Banman SL, Kary S, Stone SJ (2011) Murine diacylglycerol acyltransferase-2 (DGAT2) can catalyze triacylglycerol synthesis and promote lipid droplet formation independent of its localization to the endoplasmic reticulum. *J Biol Chem* 286: 28235 – 28246
19. Glinka A, Wu W, Delius H, Monaghan AP, Blumenstock C, Niehrs C (1998) Dickkopf-1 is a member of a new family of secreted proteins and functions in head induction. *Nature* 391: 357 – 362
20. Chamoun Z, Vacca F, Parton RG, Gruenberg J (2013) PNPLA3/adiponutrin functions in lipid droplet formation. *Biol Cell* 105: 219 – 223
21. Cerec V, Glaise D, Garnier D, Morosan S, Turlin B, Drenou B, Gripon P, Kremsdorf D, Guguen-Guillouzo C, Corlu A (2007) Transdifferentiation of hepatocyte-like cells from the human hepatoma HepaRG cell line through bipotent progenitor. *Hepatology* 45: 957 – 967
22. Parent R, Marion MJ, Furio L, Trepo C, Petit MA (2004) Origin and characterization of a human bipotent liver progenitor cell line. *Gastroenterology* 126: 1147 – 1156
23. Liscum L, Faust JR (1989) The intracellular transport of low density lipoprotein-derived cholesterol is inhibited in Chinese hamster ovary cells cultured with 3-beta-[2-(diethylamino)ethoxy]androst-5-en-17-one. *J Biol Chem* 264: 11796 – 11806
24. Stenmark H, Parton RG, Steele-Mortimer O, Lutcke A, Gruenberg J, Zerial M (1994) Inhibition of rab5 GTPase activity stimulates membrane fusion in endocytosis. *EMBO J* 13: 1287 – 1296
25. Kobayashi T, Beuchat MH, Lindsay M, Frias S, Palmiter RD, Sakuraba H, Parton RG, Gruenberg J (1999) Late endosomal membranes rich in lysobisphosphatidic acid regulate cholesterol transport. *Nat Cell Biol* 1: 113 – 118

26. Chevallier J, Chamoun Z, Jiang G, Prestwich G, Sakai N, Matile S, Parton RG, Gruenberg J (2008) Lysobisphosphatidic acid controls endosomal cholesterol levels. *J Biol Chem* 283: 27871 – 27880
27. Rosenbaum AI, Rujoi M, Huang AY, Du H, Grabowski GA, Maxfield FR (2009) Chemical screen to reduce sterol accumulation in Niemann-Pick C disease cells identifies novel lysosomal acid lipase inhibitors. *Biochim Biophys Acta* 1791: 1155 – 1165
28. Ross AC, Go KJ, Heider JG, Rothblat GH (1984) Selective inhibition of acyl coenzyme A: cholesterol acyltransferase by compound 58-035. *J Biol Chem* 259: 815 – 819
29. Heiniger HJ, Kandutsch AA, Chen HW (1976) Depletion of L-cell sterol depresses endocytosis. *Nature* 263: 515 – 517
30. Brown MS, Goldstein JL (1999) A proteolytic pathway that controls the cholesterol content of membranes, cells, and blood. *Proc Natl Acad Sci USA* 96: 11041 – 11048
31. Finkelshtein D, Werman A, Novick D, Barak S, Rubinstein M (2013) LDL receptor and its family members serve as the cellular receptors for vesicular stomatitis virus. *Proc Natl Acad Sci USA* 110: 7306 – 7311
32. Le Blanc I, Luyet PP, Pons V, Ferguson C, Emans N, Petiot A, Mayran N, Demaurex N, Fauré J, Sadoul R *et al* (2005) Endosome-to-cytosol transport of viral nucleocapsids. *Nat Cell Biol* 7: 653 – 664
33. Luyet PP, Falguieres T, Pons V, Pattnaik AK, Gruenberg J (2008) The ESCRT-I subunit TSG101 controls endosome-to-cytosol release of viral RNA. *Traffic* 9: 2279 – 2290
34. Pasqual G, Rojek JM, Masin M, Chatton JY, Kunz S (2011) Old world arenaviruses enter the host cell via the multivesicular body and depend on the endosomal sorting complex required for transport. *PLoS Pathog* 7: e1002232
35. Abrami L, Brandi L, Moayeri M, Brown MJ, Krantz BA, Leppla SH, van der Goot FG (2013) Hijacking multivesicular bodies enables long-term and exosome-mediated long-distance action of anthrax toxin. *Cell Rep* 5: 986 – 996
36. Abrami L, Lindsay M, Parton RG, Leppla SH, van der Goot FG (2004) Membrane insertion of anthrax protective antigen and cytoplasmic delivery of lethal factor occur at different stages of the endocytic pathway. *J Cell Biol* 166: 645 – 651
37. Straub BK, Herpel E, Singer S, Zimbelmann R, Breuhahn K, Macher-Goeppinger S, Warth A, Lehmann-Koch J, Longerich T, Heid H *et al* (2010) Lipid droplet-associated PAT-proteins show frequent and differential expression in neoplastic steatogenesis. *Mod Pathol* 23: 480 – 492
38. Qi W, Fitchev PS, Cornwell ML, Greenberg J, Cabe M, Weber CR, Roy HK, Crawford SE, Savkovic SD (2013) FOXO3 growth inhibition of colonic cells is dependent on intraepithelial lipid droplet density. *J Biol Chem* 288: 16274 – 16281
39. Hirsch HA, Iliopoulos D, Joshi A, Zhang Y, Jaeger SA, Bulyk M, Tsichlis PN, Shirley LX, Struhl K (2010) A transcriptional signature and common gene networks link cancer with lipid metabolism and diverse human diseases. *Cancer Cell* 17: 348 – 361
40. Daker M, Bhuvanendran S, Ahmad M, Takada K, Khoo AS (2013) Deregulation of lipid metabolism pathway genes in nasopharyngeal carcinoma cells. *Mol Med Rep* 7: 731 – 741
41. Fabricant RN, De Larco J, Todaro GJ (1977) Nerve growth factor receptors on human melanoma cells in culture. *Proc Natl Acad Sci USA* 74: 565 – 569
42. Kamentsky L, Jones TR, Fraser A, Bray MA, Logan DJ, Madden KL, Ljosa V, Rueden C, Eliceiri KW, Carpenter AE (2011) Improved structure, function and compatibility for CellProfiler: modular high-throughput image analysis software. *Bioinformatics* 27: 1179 – 1180
43. Jiao X, Sherman BT, Huang da W, Stephens R, Baseler MW, Lane HC, Lempicki RA (2012) DAVID-WS: a stateful web service to facilitate gene/protein list analysis. *Bioinformatics* 28: 1805 – 1806
44. Croft D, Mundo AF, Haw R, Milacic M, Weiser J, Wu G, Caudy M, Garapati P, Gillespie M, Kamdar MR *et al* (2014) The reactome pathway knowledgebase. *Nucleic Acids Res* 42: D472 – D477
45. D'Eustachio P (2013) Pathway databases: making chemical and biological sense of the genomic data flood. *Chem Biol* 20: 629 – 635
46. Das SC, Panda D, Nayak D, Pattnaik AK (2009) Biarsenical labeling of vesicular stomatitis virus encoding tetracysteine-tagged m protein allows dynamic imaging of m protein and virus uncoating in infected cells. *J Virol* 83: 2611 – 2622
47. Jones TR, Kang IH, Wheeler DB, Lindquist RA, Papallo A, Sabatini DM, Golland P, Carpenter AE (2008) CellProfiler Analyst: data exploration and analysis software for complex image-based screens. *BMC Bioinformatics* 9: 482
48. Pons V, Luyet PP, Morel E, Abrami L, van der Goot FG, Parton RG, Gruenberg J (2008) Hrs and SNX3 functions in sorting and membrane invagination within multivesicular bodies. *PLoS Biol* 6: e214
49. Gruenberg J, Griffiths G, Howell KE (1989) Characterization of the early endosome and putative endocytic carrier vesicles *in vivo* and with an assay of vesicle fusion *in vitro*. *J Cell Biol* 108: 1301 – 1316
50. Barrett T, Wilhite SE, Ledoux P, Evangelista C, Kim IF, Tomashevsky M, Marshall KA, Phillippy KH, Sherman PM, Holko M *et al* (2013) NCBI GEO: archive for functional genomics data sets–update. *Nucleic Acids Res* 41: D991 – D995
51. Davis S, Meltzer PS (2007) GEOquery: a bridge between the Gene Expression Omnibus (GEO) and Bioconductor. *Bioinformatics* 23: 1846 – 1847
52. Smyth GK (2005) Limma: linear models for microarray data. In Gentleman R, Carey V, Dudoit S, Irizarry R and Huber W (eds.), *Bioinformatics and Computational Biology Solutions using R and Bioconductor*, chapter 23, pp. 397 – 420. Springer, New York
53. Bolstad BM, Irizarry RA, Astrand M, Speed TP (2003) A comparison of normalization methods for high density oligonucleotide array data based on variance and bias. *Bioinformatics* 19: 185 – 193
54. Jensen LJ, Kuhn M, Stark M, Chaffron S, Creevey C, Muller J, Doerks T, Julien P, Roth A, Simonovic M *et al* (2009) STRING 8–a global view on proteins and their functional interactions in 630 organisms. *Nucleic Acids Res* 37: D412 – D416
55. Brankatschk B, Wichert SP, Johnson SD, Schaad O, Rossner MJ, Gruenberg J (2012) Regulation of the EGF transcriptional response by endocytic sorting. *Sci Signal* 5: ra21

